

Acoustic Emission Analysis of Polymer Electrolyte Membrane Fuel Cells

V.S. Bethapudi^{a, b}, G. Hinds^c, P.R. Shearing^b, D.J.L. Brett^{b,*} and M.-O. Coppens^{a,**}

^a EPSRC “Frontier Engineering” Centre for Nature Inspired Engineering, Department of Chemical Engineering, University College London, London WC1E 7JE, United Kingdom

^b Electrochemical Innovation Lab, Department of Chemical Engineering, University College London, London WC1E 7JE, United Kingdom

^c National Physical Laboratory, Hampton Road, Teddington, Middlesex, TW11 0LW, United Kingdom

The performance of a polymer electrolyte membrane fuel cell (PEMFC) is characterized using acoustic emission (AE) based analysis. Polarization scans indicate that an increase in cell temperature from 45 °C to 60 °C results in a drop in maximum current density due to cell dehydration. Parametric analysis of acoustic activity generated from the PEMFC during polarization establishes a relationship between the cell operating conditions and the corresponding AE generated. Optimal and dehydrated cell conditions result in stable and reduced numbers of generated acoustic events, respectively, which are related to the flow of water and its physical state in the flow-fields. Furthermore, the AE parameters utilized for hydration analysis are amplitude and counts, which correspond to intensity and proportion of AE generated beyond a threshold, respectively; these are influenced by current density, reactant humidity and cell temperature.

Introduction

Understanding water management is critical in evaluating the performance, durability and behaviour of polymer electrolyte membrane fuel cells (PEMFCs) (1). Water inside a PEMFC results primarily from the humidity carried by reactants, and the product water generated from the electrochemical reaction at the cathode. Sufficient water retention inside a PEMFC ensures proper membrane hydration and its associated conductivity (2,3). Improper hydration can result in poor performance; under dehydrated conditions especially, proton conductivity of the membrane reduces significantly and degradation of the membrane can occur (4).

The performance of a PEMFC is a good indicator of the state of water distribution inside it. For instance, dehydration in a PEMFC is indicated, indirectly, by reduced polarization performance and increased Ohmic resistance (5,6). However, direct evaluation and quantification of water distribution inside a PEMFC will aid in understanding the role of physical and design parameters of the cell on the water distribution dynamics inside the cell. In this context, effective direct water evaluation inside PEMFCs has been achieved using techniques like X-ray radiography (7,8), X-ray computed tomography (9,10), neutron radiography (11,12) and optical photography

(13,14). However, these techniques have certain limitations, such as complexity in operation, radiation exposure, accessibility, cost, and restricted material use.

Acoustic activity from a system is measured as acoustic emission (AE), which occurs when elastic waves are generated from a material undergoing mechanical perturbation. AE is used for monitoring, diagnostics, analytical and other related studies in a wide range of fields, varying from corrosion science (15) to medical physics (16), the automotive industry (17), and construction materials (18). In the field of electrochemical science and engineering, AE has been utilized for diagnostics in several applications. For fuel cells, so far, AE has been utilized as a non-destructive technique for fault analysis and diagnosis (19), thermo-mechanical characterization of solid oxide fuel cells (SOFCs) (20), damage evaluation of SOFCs (21), monitoring structural properties during drying and swelling of Nafion membrane (22) and diagnosis of physicochemical changes occurring inside a PEMFC under various operating conditions (23). Recently, Bethapudi et al. (24) developed acoustic emission as a function of polarization (AEfP), as a technique to probe the water dynamics inside a PEMFC, by measuring the AE energy released from the cell at discrete points of polarization. Furthermore, the measured AE energy was utilized for correlating the level of cell polarization with the liquid water generation and removal within flow-fields. This study (24) was instrumental in evaluating the performance of two different fractal flow-field PEMFCs, reported in Bethapudi et al. (25), where flooding and normal operating conditions were diagnosed in 2-way and 1-way fractal flow-fields, respectively, using AE metrology.

Building on this work, we here report on the analysis of the performance of a PEMFC on the basis of the generation and distribution of AE parameters associated with liquid water release into flow-fields. Furthermore, the intensity and amount of water impacting the flow-fields has been quantified using AE signal parameters, namely amplitude and counts.

Experimental

The PEMFC utilized in this study was developed from layered printed circuit board (PCB) plates, using a methodology outlined in (26). The cathode and anode flow-fields had a single-serpentine 1 mm^2 square channel arrangement with a depth of 1 mm, covering an active membrane electrode assembly (MEA) area of 6.25 cm^2 . The MEA was developed using a non-reinforced Nafion[®] 212 membrane (DuPont, USA) and $0.4 \text{ mg}_{\text{Pt}}\text{cm}^{-2}$ Pt/C (HyPlat, South Africa) electrodes. The cells were preheated to set temperatures using heating cartridges. The overall cell assembly components and details can be obtained from a previous article (24). The fuel cell testing was carried out on a Scribner 850e test station, and the corresponding hydrogen and air flow rates were maintained constant at 100 mL min^{-1} of hydrogen and 500 mL min^{-1} of air, respectively. The polarization scans were performed between open circuit voltage (OCV) and 0.3 V cell voltage, at 0.05 V intervals, with 30 s hold at each voltage interval point. Further details of the test station and polarization conditions are given in (24).

The AE setup utilized in this study was a piezoelectric based transducer sensor (S9208; Mistras NDT, UK). The sensor's resonant and operating frequency range were 500 kHz and 200 kHz – 1000 kHz, respectively. The threshold amplitude considered here was 27 dB, based on the background and operating noise generated during cell operation.

In addition, the acoustic sensor was fastened against the cathode flow-field plate, where more water is generated during fuel cell operation. In this study, the key acoustic parameters measured from the AE signals were peak amplitude (dB) and peak counts. The acoustic parameters were recorded simultaneously with the fuel cell operation. Further details on the parametric understanding of the AE hit are given in (24).

Results & Discussion

Polarization performance of the PEMFC at optimal (45°C) and higher (60°C) cell set temperatures and at 40%, 70% and 100% reactant relative humidity (RH) are given in Fig. 1. It can be observed that, irrespective of cell set temperature, the cell performance increased with an increase in the reactant RH as a result of increased membrane hydration at higher reactant RH. However, the cell performance at corresponding voltage points on the polarization curves decreased with an increase in temperature; an increase by 15°C resulted in a drop in maximum current density by 52% at 40% RH, 50% at 70% RH and 35% at 100% RH, as a result of cell dehydration. Cell dehydration at 60°C was confirmed by the larger Ohmic resistances measured, which were $\sim 30\%$ larger than those measured at 45°C , as reported in (24).

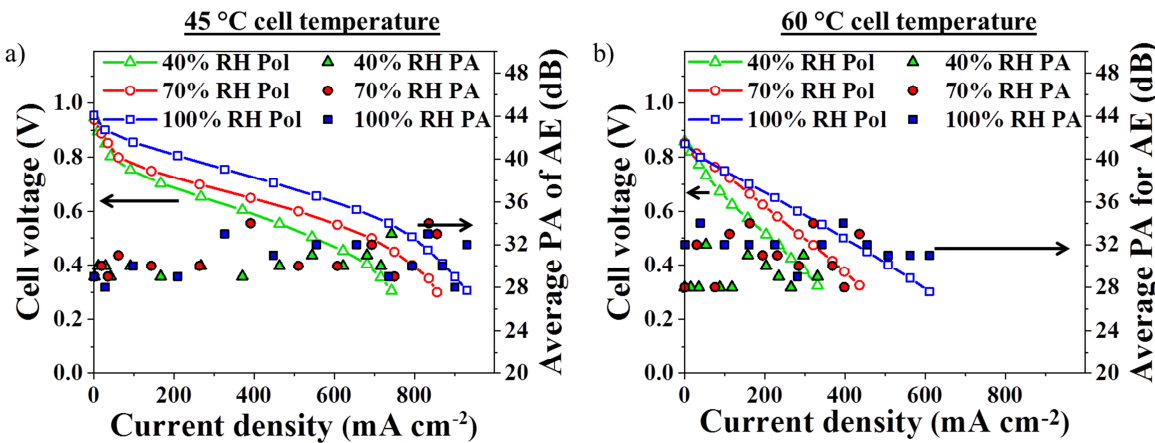


Figure 1: Average of the peak amplitude (PA) developed for the AE generated during cell polarization, at (a) 45°C and (b) 60°C cell set temperatures. PA represents the intensity of AE generated as a result of liquid water impacting the flow-field. Legend: RH – relative humidity; Pol – polarization; PA – peak amplitude.

It has been identified that acoustic activity from PEMFCs can be utilized to establish the hydration conditions inside the fuel cell, as reported in (24,25). Physical impact events created by the release of water into flow-fields result in the generation of AE and the corresponding intensity of such impacts is measured by the amplitude (dB) of AE signals detected. Furthermore, peak amplitude (PA) corresponds to the largest of the amplitudes detected in an AE signal, above a threshold value, which defines the overall energy of the AE signal (23,24). It can be observed from Fig. 1 that, irrespective of cell conditions, the average PA of the AE signals measured during the polarizations was between $28 - 35$ dB, indicating a fixed impact range from liquid water release into flow-fields. Such a confined amplitude range is consistent with the measured AE signal being

associated with water impacts occurring specifically in the flow-fields (23,24), which have a fixed physical dimension defining their magnitude. Furthermore, the amount of liquid water generated inside the cell can be evaluated from the peak counts in an AE signal, which reflects the number of times a PA associated with water impacts has been detected. It can be observed from Figs. 2 and 3 that the counts increased with an increase in the reactant RH, irrespective of cell temperature, which can be attributed to the greater amount of liquid water generated inside the cell from condensation (23,24). In addition, it can be observed from Fig. 2 (a – c) that the counts tended to increase with current density, which is due to increased water generation from the electrochemical reaction. However, the counts decreased significantly when the cell set temperature was increased to 60 °C, as shown in Fig. 3, as a result of the lower amounts of liquid water released into the flow-field, due to the reduced rate of condensation at the higher temperature.

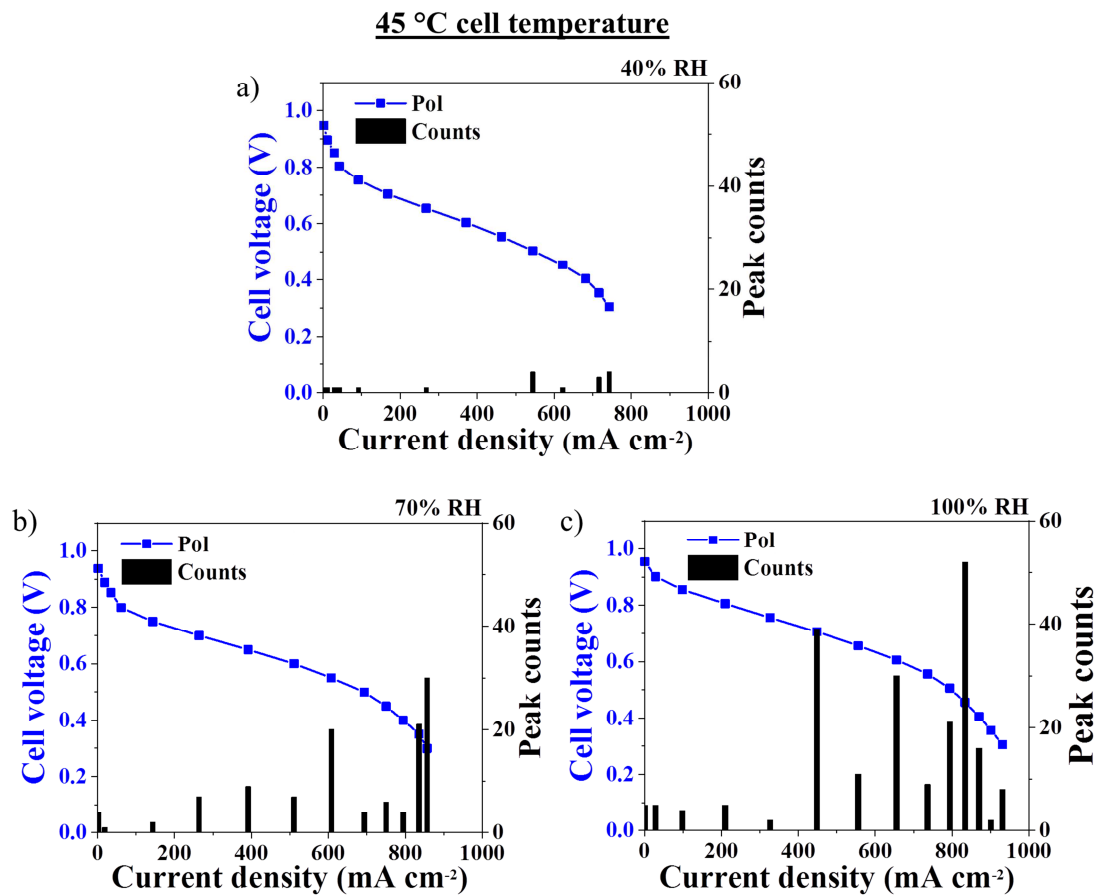


Figure 2: Peak counts – a measure of the number of peak amplitudes (PAs) generated – during cell polarization for a cell set temperature of 45 °C at (a) 40% RH, (b) 70% RH, (c) 100% RH. Legend: Pol – polarization.

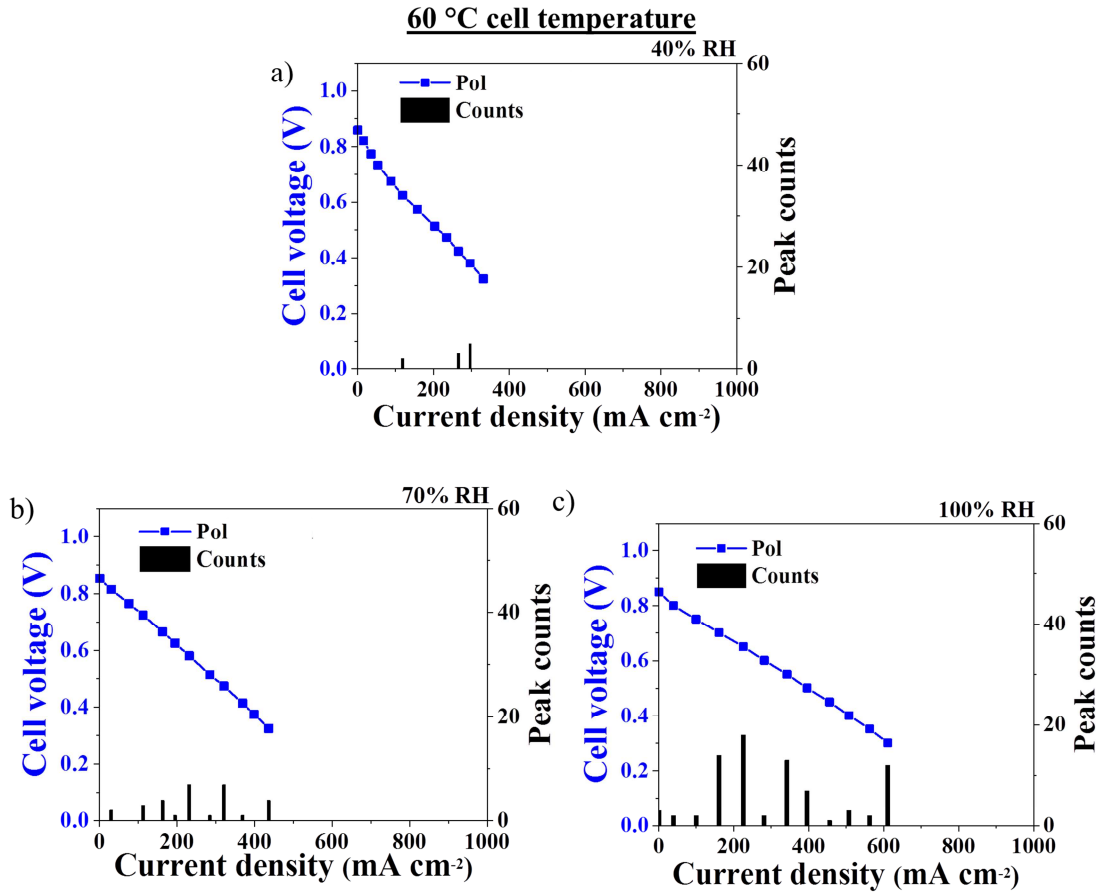


Figure 3: Peak counts – a measure of the number of peak amplitudes (PAs) generated – during cell polarization for a cell set temperature of 60 °C at (a) 40% RH, (b) 70% RH, (c) 100% RH. Legend: Pol – polarization.

Furthermore, the corresponding cell temperature evolution during polarization as a function of reactant RH and cell set temperature is shown in Fig. 4.

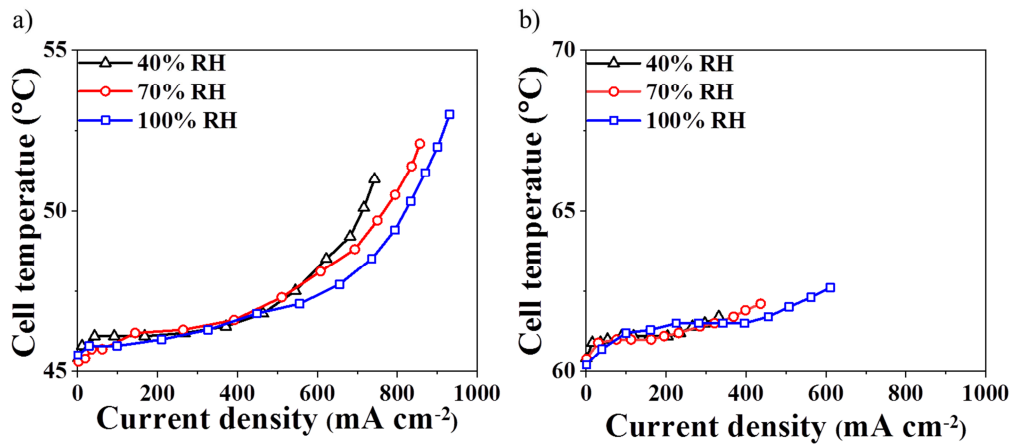


Figure 4: Cell temperature evolution during polarization at 40%, 70% and 100% reactant RH conditions, at (a) 45 °C and (b) 60 °C cell set temperature.

Higher cell set temperatures resulted in a decrease in OCV, as seen in Fig. 1, which is likely due to the reduced mass fractions of hydrogen and oxygen at the higher temperature (27). Furthermore, it can be observed that at 45 °C cell set temperature, the maximum cell temperatures attained at 40% RH, 70% RH and 100% RH conditions were ~51 °C, ~52 °C and ~53 °C, respectively, and the corresponding maximum current densities were ~740 mA cm⁻², ~860 mA cm⁻² and ~930 mA cm⁻², respectively, while at 60 °C set temperature the maximum cell temperatures attained at 40% RH, 70% RH and 100% RH conditions were ~61 °C, ~62 °C and ~63 °C, respectively, and the corresponding maximum current densities were ~330 mA cm⁻², ~440 mA cm⁻² and ~610 mA cm⁻², respectively. The current density determines both the increase in cell temperature and the amount of water generated. A similar temperature rise was observed for cell set temperatures of 45 °C and 60 °C, when comparing points at the same current density, as seen in Figs. 2 and 3. However, the maximum rise in cell temperature of ~1 – 3 °C at 60 °C, as opposed to ~6 – 8 °C at 45 °C, can be attributed to the reduced performance (maximum current density) delivered by the cell at 60 °C, which also resulted in lower amounts of liquid water generated, as shown in (Fig. 3(a – c)).

Galvanostatic tests were performed on the PEMFC at a constant current hold of 600 mA cm⁻² and 45 °C cell set temperature for ~300 s. The corresponding PA and peak counts as a function of time during the current hold are shown in Figs. 5(a) and 5(b), respectively. Fig. 5(a) shows that, at each tested reactant RH, the PA between 0–25 s reached peaks up to 50 dB, which is higher than the aforementioned steady-state range of about 28–35 dB. This can be attributed to the cell stabilization period before a steady-state develops that is determined by the reactant flow rate, temperature and humidity (23).

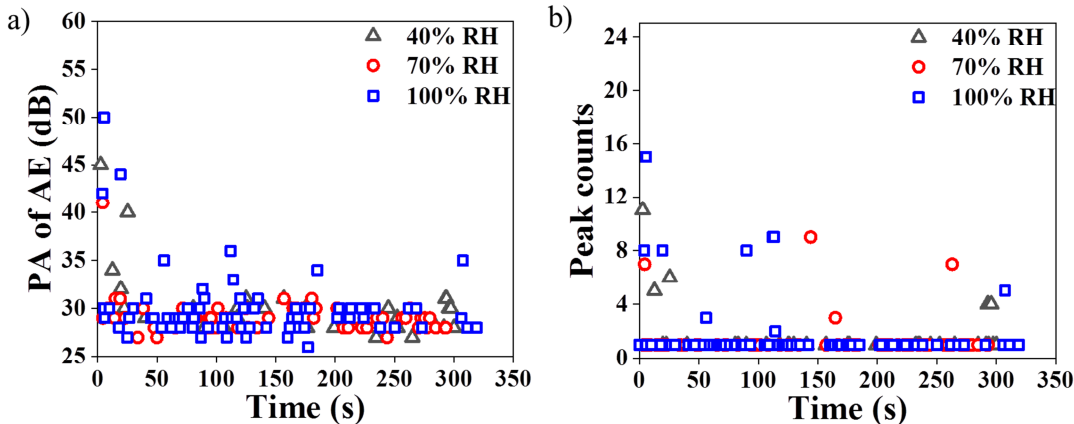


Figure 5: (a) PA of AE and (b) peak counts developed during galvanostatic tests on the PEMFC at 45 °C cell set temperature and 600 mA cm⁻² for ~300 s.

Beyond 50 s, the observed PA for all conditions again ranged between 28 – 35 dB, confirming the impact generation occurring from liquid water release into the flow-fields, similar to that shown in Fig. 1. However, under 100% RH conditions, intermittent large PA values were detected, which can be attributed to excess hydration and its associated water condensation and release into the cell, resulting in flushing events. Flushing events occur when water droplets generated inside a PEMFC and released into the flow-fields

coalesce as large droplets and are eventually expelled from the fuel cell, resulting in large AE (24). Furthermore, the peak counts during current hold, as shown in Fig. 5(b), indicate an initial spike in the initial, 0 – 25 s period, which can be attributed to stabilization, similar to that observed in Fig. 5(a) for the PA values. In addition, the counts measured increased with an increase in the reactant RH. However, at 40% RH, the number of peak counts was considerably lower, which can be attributed to reduced liquid water generation inside the cell at this low RH. At higher reactant RH, the hydration levels improved inside the cell, which was reflected in better cell performance (reduced Ohmic resistances as shown in Fig. 4 of Bethapudi et al. (24)) and increased water generation from electrochemical reaction, as in Fig. 1(a), resulting in more counts.

Conclusions

This study reported the evaluation of hydration conditions inside a PEMFC at a range of operating and reactant conditions by measuring the acoustic activity generated from the cell. A good correlation was found between acoustic emission (AE) and cell performance. The hydration conditions inside the cell were categorized into peak amplitudes (PA) and peak counts of AE, which were identified via the intensity and size of AE events occurring inside the cell. A narrow, fixed range in PA of AE events observed during cell polarizations, irrespective of reactant RH and cell condition, confirmed that the AE was primarily generated through liquid water droplet impacts occurring in the flow-fields. In addition, lower peak count numbers were developed during low reactant humidity conditions (40% RH), as a result of dehydrated cell conditions, which was corroborated by the corresponding polarization performance. An increase in reactant RH to 70% RH and 100% RH resulted in a larger number of counts and improved cell performance, confirming that the amount of liquid water generated inside the cell has a direct influence on acoustic activity and cell performance, and *vice versa*. Furthermore, galvanostatic tests provided corroborative evidence for the influence of discrete and cumulative effects of operating conditions and reactant RH on the acoustic activity generated from a fuel cell.

Acknowledgments

The authors would like to acknowledge funding from the EPSRC “Frontier Engineering: Progression” Award (EP/S03305X/1), and other funds from the EPSRC for supporting fuel cell research in the “Electrochemical Innovation Lab (EIL)” (EP/R023581/1, EP/P009050/1, EP/L015749/1, EP/M014371/1, EP/M023508/1, EP/M009394/1). We also thank the Department of Chemical Engineering, University College London, and the National Measurement System of the UK Department of Business, Energy and Industrial Strategy for supporting this work. The authors would like to acknowledge Dr. Quentin Meyer and Professor Daniel Steingart for their assistance in sourcing the equipment and supplying the interfacing code used to obtain the data.

References

1. Yang, D., Wang, H., Ma, J., Dai, W., Yuan, X.-Z., Martin, J. J., & Qiao, J. **International Journal of Hydrogen Energy**. 34: 9461–9478, 2009.
2. Nasef, M. M. & Aly, A. A. **Desalination**. 287: 238–246, 2012.
3. Lim, B. H., Majlan, E. H., Daud, W. R. W., Husaini, T., & Rosli, M. I. **Ionics**. 22:

- 301–316, 2016.
- 4. Weng, F. B., Jou, B. S., Li, C. W., Su, A., & Chan, S. H. **Journal of Power Sources**. 181: 251–258, 2008.
 - 5. Song, Y., Xu, H., Wei, Y., Kunz, H. R., Bonville, L. J., & Fenton, J. M. **Journal of Power Sources**. 154: 138–144, 2006.
 - 6. Sone, Y. **Journal of The Electrochemical Society**. 143: 1254, 1996.
 - 7. Chevalier, S., Ge, N., Yip, R., Antonacci, P., Bazylak, A., & Lee, J. **International Journal of Hydrogen Energy**. 40: 16494–16502, 2015.
 - 8. Rahimian, P., Zhang, L., Battrell, L., Anderson, R., Zhu, N., & Johnson, E. **Experimental Thermal and Fluid Science**. 97: 237–245, 2018.
 - 9. Alrwashdeh, S. S., Markotter, H., Haussmann, J., Hilger, A., Manke, I., & Scholta, J. **ECS Transactions**. 72: 99–106, 2016.
 - 10. Zenyuk, I. V., Parkinson, D. Y., Hwang, G., & Weber, A. Z. **Electrochemistry Communications**. 53: 24–28, 2015.
 - 11. Cho, J. I. S., Neville, T. P., Trogadas, P., Bailey, J., Shearing, P., Brett, D. J. L., & Coppens, M. O. **International Journal of Hydrogen Energy**. 43: 21949–21958, 2018.
 - 12. Wu, Y., Cho, J. I. S., Neville, T. P., Meyer, Q., Zeische, R., Boillat, P., Cochet, M., Shearing, P. R., & Brett, D. J. L. **Journal of Power Sources**. 399: 254–263, 2018.
 - 13. Guo, N., Leu, M. C., & Koylu, U. O. **International Journal of Hydrogen Energy**. 39: 21185–21195, 2014.
 - 14. Bozorgnezhad, A., Shams, M., Kanani, H., Hasheminasab, M., & Ahmadi, G. **International Journal of Hydrogen Energy**. 40: 2808–2832, 2015.
 - 15. Skal's'kyi, V. R., Nazarchuk, Z., Dolins'ka, Y., Yarema, R. Y., & Selivonchyk, V. **Materials Science**. 53: 295–305, 2017.
 - 16. Kiselev, J., Ziegler, B., Schwalbe, H. J., Franke, R. P., & Wolf, U. **Medical Engineering and Physics**. 65: 57–60, 2019.
 - 17. Brokmann, C., Alter, C., & Kolling, S. **Glass Structures and Engineering**. 4: 229–241, 2019.
 - 18. Grazzini, A., Accornero, F., Lacidogna, G., & Valente, S. **Construction and Building Materials**. 236: 117798, 2020.
 - 19. Benmouna, A., Becherif, M., Depernet, D., Gustin, F., Ramadan, H. S., & Fukuhara, S. **International Journal of Hydrogen Energy**. 42: 1534–1543, 2017.
 - 20. Malzbender, J. & Steinbrech, R. W. **Journal of Power Sources**. 173: 60–67, 2007.
 - 21. Dev, B., Walter, M. E., Arkenberg, G. B., & Swartz, S. L. **Journal of Power Sources**. 245: 958–966, 2014.
 - 22. Legros, B., Nogueira, R. P., Thivel, P.-X., Bultel, Y., & Boinet, M. **Electrochemical and Solid-State Letters**. 12: B116, 2009.
 - 23. Legros, B., Thivel, P. X., Bultel, Y., Boinet, M., & Nogueira, R. P. **Journal of Power Sources**. 195: 8124–8133, 2010.
 - 24. Bethapudi, V. S., Maier, M., Hinds, G., Shearing, P. R., Brett, D. J. L., & Coppens, M. O. **Electrochemistry Communications**. 109: 106582, 2019.
 - 25. Bethapudi, V. S., Hack, J., Trogadas, P., Hinds, G., Shearing, P. R., & Brett, D. J. L. **Energy Conversion and Management**. 220: 113083, 2020.
 - 26. Bethapudi, V. S., Hack, J., Trogadas, P., Cho, J. I. S., Rasha, L., Hinds, G., Shearing, P. R., Brett, D. J. L., & Coppens, M.-O. **Energy Conversion and Management**. 202: 112198, 2019.
 - 27. Zhang, J., Tang, Y., Song, C., Zhang, J., & Wang, H. **Journal of Power Sources**. 163: 532–537, 2006.